High Stability and Sensitivity Correlation Polarimeters for CMB Polarization Measurements

E. Carretti[a], S. Cortiglioni[a], C. Macculi[a], C. Sbarra[a], G. Ventura[a],
J. Monari[b], M. Poloni[b], S. Poppi[b],
V. Natale[c], R. Nesti[c],
M. Baralis[d], O. Peverini[d], R. Tascone[d], G. Virone[d],
G. Sironi[e], M. Zannoni[f,e]

[a]CNR-IASF Bologna, Via Gobetti 101, I-40129, Bologna, Italy
[b]CNR-IRA Bologna, Via Gobetti 101, I-40129, Bologna, Italy
[c]CNR-IRA Firenze, Largo E. Fermi 5, I-50125 Firenze, Italy
[d]CNR-IEIIT, C.so Duca degli Abbruzzi 24, I-10129 Torino, Italy
[e]Universitá di Milano - Bicocca, P.zza della Scienza 3, I-20126 Milano, Italy
[f]CNR-IASF Milano, Via Bassini 15, I-20133 Milano

ABSTRACT

The measure of the faint polarized signal of the Cosmic Microwave Background (few percent of the CMB Anisotropy) requires instruments with very low contamination from systematic effects, high stability and high sensitivity. The BaR-SPOrt experiment, in sharing with the SPOrt project on ISS, is based on analog correlation receivers with components custom designed to match all of these requirements. Here we present the architecture, the design analysis and the status of the realization of the 32 GHz receiver.

Keywords: Instrument, Polarimeter, Polarization, Radioastronomy, Cosmic Microwave Background

1. BAR-SPORT: THE SCIENTIFIC CONTEST AND EXPERIMENT

After the precise detection of the anisotropies of the Cosmic Microwave Background (CMB) done with the WMAP's first year data[1–3] and in view of the even finer measurements foreseen for the WMAP's 4 year operations and the PLANCK mission,[4] the next challenge for CMB scientists is represented by the CMB Polarization (CMBP).

The science allowed by CMBP promises to be very exciting. Besides solving the degeneracy among cosmological parameters left by CMB anisotropy alone, CMBP allows the investigation of the epoch of Galaxy and star formation through the signature left by the reionization history of the Universe on the polarization power spectra (e.g. see Ref. 5–7).

On sub-degree angular scales, the Inflation scenario foresees that the E-mode spectrum of the polarization is featured by a peak pattern related to that already detected for the anisotropy: maxima of the E-mode correspond to minima in anisotropy and reverse (eg. see Figure 1 and Ref. 9). A full characterization of the E-mode on small angular scales is thus important to check the inflationary frame.

Much more intriguing is the second component of CMBP: although orders of magnitude fainter than the E-mode, the B-mode brings information on the gravitational wave background generated in the early stage of the Universe and can give us a direct insight to the Inflation era.[10,11] The B-mode is generated only by tensorial perturbation and its detection would be a clear evidence of a gravitational wave background. Moreover, the level of this signal is proportional to the energy density at the Inflation epoch, providing us information on when Inflation occurred.

Further author information: (Send correspondence to E. Carretti)
E. Carretti: E-mail: carretti@bo.iasf.cnr.it

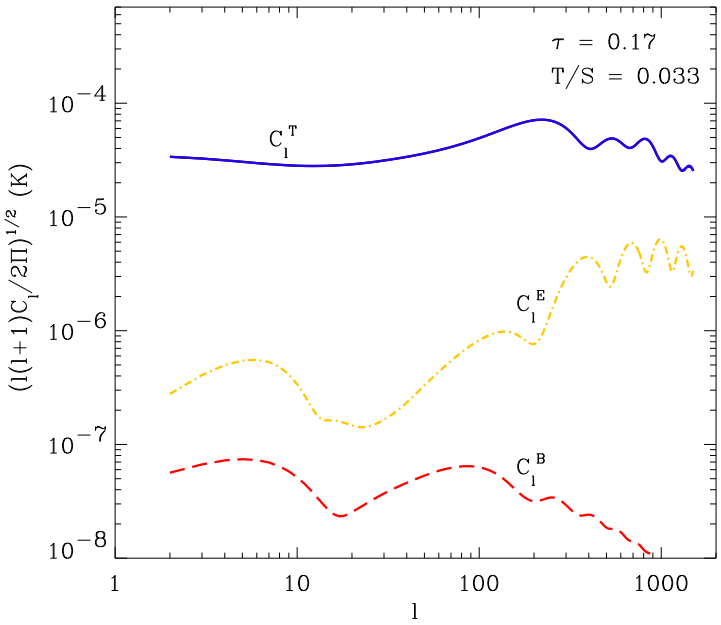

Figure 1. Power spectra of anisotropy, E- and B-modes of the CMB (C_ℓ^T, C_ℓ^E, C_ℓ^B, respectively). The quantity $\sqrt{\ell(\ell+1)\,C_\ell/2\pi}$ is a fair estimate of the signal at angular scale $\theta = 180^\circ/\ell$. The cosmological parameters used for these spectra are as from the WMAP's first year results[8] along with a scalar-to tensor power ration $T/S = 0.03$.

In spite of its importance, CMBP is weak (see Figure 1, where it is compared to the CMB anisotropy) and its measurement is a challenge for both micro- and millimeter-wave polarimeters. In fact, CMBP measurements are just at the beginning with the first measurements of the E-mode announced in the last two years,[12,13] and a full characterization of its spectrum is still far from having been done. Moreover, the B-mode is still elusive and far from the capability of present instruments.

Thus, the extremely week CMBP signal requires instruments optimized to keep under control systematics and spurious signals. In fact, high sensitivity measurements require low systematics and high stability to effectively benefit of long integration times and good istantaneous sensitivities.

The Balloon-borne Radiometers for Sky Polarization Observations (BaR-SPOrt) is an experiment devoted to measure the linearly polarized emission of the CMB. Its design, based on radio-polarimeters in the 30-90 GHz range and in sharing with the space experiment SPOrt,[14] has been optimized to minimize sytematics effects and have a high purity in Q and U Stokes parameter measurements.

Here we present the design and the development status of the 32 GHz instrument, the first to be completed and ready to observe next year (2005).

The 32 GHz instrument consists of a polarimetric receiver coupled to a on-axis 1.8 m Cassegrain optics to

Table 1. BaR-SPOrt 32 GHz main features: BW is the banwidth, FWHM the angular resolution and σ_{1s} the 1 second sensitivity.

ν [GHz]	BW	FWHM	Scan Time [min]	σ_{1s} [μKs$^{1/2}$]
32	10%	0.4°	1-2	500

Figure 2. View of the 32 GHz receiver coupled to the 1.8 m Cassegrain optics. The dielectric window closing the vacuum chamber of the receiver is visible at the horn mouth.

provide an angular resolution of 0.4°. Figure 2 shows a view of the receiver together with the mirror optics, while the main specifications are reported in Table 1.

The main scientific goal is to map the polarized emission in a small sky patch to measure the power spectrum of the CMBP E-mode up to the $\ell = 50$–400 multipole range*. Figure 3 shows its capability, reporting error boxes in the ℓ-space for a 6 month observation of a $6^\circ \times 6^\circ$ region.

The region will be observed through horizontal scans performed in 1-2 min. This modulation of the sky signal allows destriping techniques to remove the receiver instabilities on time scales longer than the scan duration, so that what does matter is to assure the stability within this period (e.g. see Ref. 15 and references therein).

2. BAR-SPORT RECEIVER DESIGN

2.1. Architecture

Among the possible architectures to directly measure the Stokes parameters, we use the correlation of the Left- and Right-Handed circular polarizations E_L and E_R. With respect to the other schemes proposed to date, it has the advantage to detect simultaneously both Q and U as

$$\begin{aligned} Q &= \Re(E_R \cdot E_L^*), \\ U &= \Im(E_R \cdot E_L^*). \end{aligned} \tag{1}$$

The other schemes, instead, can provide just one of them at once. In fact, the correlation of the two linear polarizations E_X and E_Y, like for PIQUE,[16] POLAR,[17] COMPASS[18] and CAPMAP[19] experiments, provides just U

$$U = \Re(E_X \cdot E_Y^*), \tag{2}$$

*The multipole ℓ is the angular frequency in the spherical harmonics space and is related to the angular scale θ through $\theta = 180^\circ/\ell$.

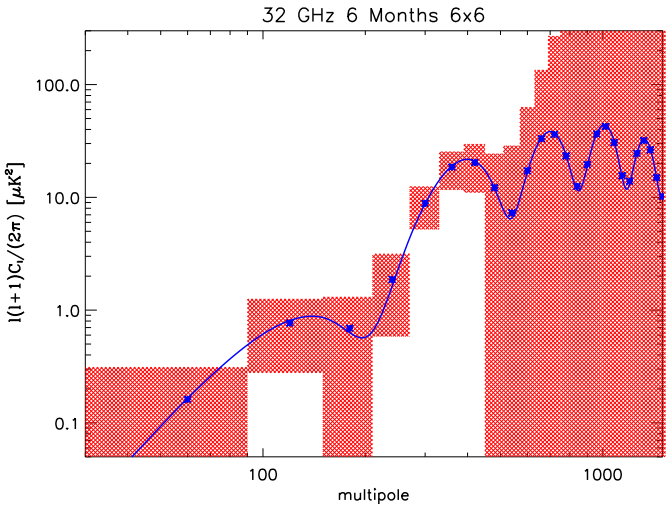

Figure 3. E-mode power spectrum expected for CMBP together with the error boxes achivable by the 32 GHz instrument in 6-month observations of a $6^\circ \times 6^\circ$ area. We use the latest cosmological paramter set as from WMAp's results.[8]

leading to a loss of 50% in time-efficiency (Q is measured by rotating the instrument by 45°, and the experiment can spend just half of the time for each of the two Stokes parameters).

Similar considerations can be done also for the Total Power schemes (e.g. WMAP and PLANCK), that provides just Q by detecting directly $|E_X|^2$ and $|E_Y|^2$,

$$Q = \frac{|E_X|^2 - |E_Y|^2}{2}. \tag{3}$$

It is worth noting that in this case the measurement is not direct, but it is performed off-line after the measurements of the two polarizations.

Beside the loss of efficiency, the last two schemes deal with Q and U detected from different receivers, adding the problem to well match independent calibrations before coupling these two related quantities.

Referring to Figure 4, the correlation scheme of BaR-SPOrt is realized as follows: the two circular polarizations collected by a feed horn are extracted by a polarizer and an OMT. After the amplification performed by HEMT, the signal is correlated by the Correlation Unit (CU) based on a Hybrid Phase Discrimanator[20] (HPD), diodes and differential amplifiers (see Ref. 14 for details) which performs the products of Equation (1).

In terms of thermal environments, the 32 GHz receiver is divided into three rooms (see Ref. 21 for further details):

- the horn: It is kept at room temperature ($T_{\rm ph}^{\rm horn} \sim 300$ K) and is actively controlled through heaters within $\Delta T_{\rm ph}^{\rm horn} = \pm\, 0.1$ K (peak-to-peak).
- polarizer, OMT, and the first amplification stage: They are kept at cryogenic temperature ($T_{\rm ph}^{\rm cold} \sim 70 - 80$ K) to improve the noise temperature $T_{\rm sys}$. The cooling is provided by a mechanical mini cryo-cooler, with a closed-loop control assuring a stability within $\Delta T_{\rm ph}^{\rm cold} = \pm\, 0.1$ K (peak-to-peak).
- the second amplification stage along with the CU and the Low Frequency (LF) electronics: They are at room temperature too ($T_{\rm ph}^{\rm warm} \sim 300$ K) and also in this case the temperature is actively controlled through heaters within $\Delta T_{\rm ph}^{\rm warm} = \pm\, 0.1$ K (peak-to-peak).

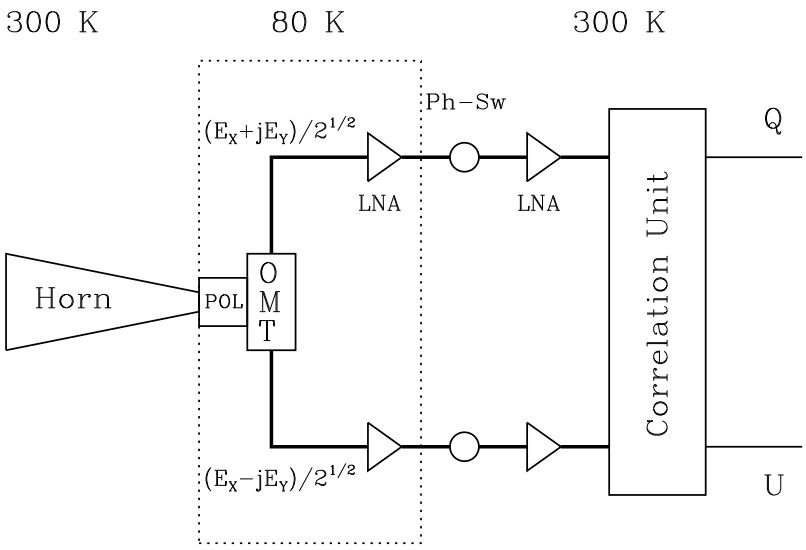

Figure 4. Schematics of the BaR-SPOrt receiver correlating the two circular polarization of the incoming radiation. The relevant components are shown together with the three thermal environments of the 32 GHz receiver: the horn at $\sim$ 300 K; the rest of the antenna system and the first LNA stage at $\sim$ 80 K; the warm RF and the LF electronics at $\sim$ 300 K again.

2.2. 1/f Noise Receiver Instabilities

One major problem to be faced with a radiopolarimeter at tens of GHz is the high level of $1/f$ noise of the Low Noise Amplifiers (LNAs). The InP technology allows impressive performances in terms of white noise,[22] but is featured by a low stability level. This is generally measured by the *knee* frequency $f_{\rm knee}^{\rm LNA}$, that, defined in the power spectrum domain as the frequency at which the $1/f$ noise component equals the white one, gives the time scale at which the instabilities become relevant. In math terms, $f_{\rm knee}^{\rm LNA}$ is defined through the equation of the noise power spectrum $P(f)$

$$P(f) = \sigma_0^2 \left[1 + \left(\frac{f_{\rm knee}^{\rm LNA}}{f}\right)^{\alpha}\right] \tag{4}$$

where σ_0 is the 1-second sensitivity and $\alpha \sim 1$ the spectral index of the $1/f$'s power law behaviour.

The knee frequency $f_{\rm knee}$ of a receiver, instead, is related to that of its amplifiers by the formula[24]

$$f_{\rm knee} = \left(\frac{T_{\rm offset}}{T_{\rm sys}}\right)^{2/\alpha} f_{\rm knee}^{\rm LNA} \tag{5}$$

where $T_{\rm offset}$ is the offset level, $T_{\rm sys}$ the system noise temperature and $f_{\rm knee}^{\rm LNA}$ the knee frequency of the amplifier. In practice, the offset is a correlated signal generated by the instrument itself when observing an unpolarized source and it is also called *instrumental polarization*.

Since a typical value of InP devices is $f_{\rm knee}^{\rm LNA} \sim 1$ kHz (see Ref. 23), total power systems are not suitable for high sensitivity experiments, characterized by long integration time. Correlation (or pseudo-correlation) schemes, with lower offset generation, are much more suitable.

The analysis of Ref. 25 identifies in the antenna assembly the leading offset source for correlation polarimeters. In particular it is found that the instrumental polarization is mainly generated by the differential attenuation between the two polarizations of the polarizer and by the cross-talk between the two OMT arms.

To reach a high level of purity, these two *critical* components have been custom realized reaching very high performances well above the present state-of-the-art in terms of instrumental polarization generation (see Ref. 26). In particular, for the 32 GHz receiver, the following requirements have been satisfied:

- differential attenuation between the two polarizations of the polarizer of

$$|A_{\parallel} - A_{\perp}| \sim -30\,\mathrm{dB}, \tag{6}$$

  corresponding to a rejection of the unpolarized component of $\sim 5 \times 10^{-4}$;

- cross-talk between the two OMT arms of about -65 dB and isolation of about 70 dB, corresponding to a rejection of the unpolarized component of $\sim 1 \times 10^{-3}$.

This corresponds to an offset of[25]

$$T_{\mathrm{offset}} \sim 50\,\mathrm{mK}. \tag{7}$$

Considering $T_{\mathrm{sys}} \sim 40$ K and $f_{\mathrm{knee}}^{\mathrm{LNA}} \sim 50$ Hz as typical values for InP LNAs in Ka band when cooled down to 80 K, our system should feature a

$$f_{\mathrm{knee}} \sim 7 \times 10^{-5}\,\mathrm{Hz}, \tag{8}$$

providing a suitable stability with wide margins over the scan duration (1-2 min).

The other part of the radiometer generating instrumental polarization is the Correlation Unit, whose core is a waveguide HPD.[20] Mixing the input signals to provide their combinations, some leakage occurs, generating contamination of the unpolarized component into Q and U. Also in this case, to have high performances, we have developed a custom designed HPD aimed at assuring a contamination below -30 dB.

A further reduction of the offset generated by CU can be achieved inserting it in a lock-in ring. A $0° - 180°$ phase modulator just before the HPD allows to alternately change the sign of Q and U, while leaving untouched the residual offset of CU. A demodulator after the CU allows to recover the signal and cancel the residual offset. In general, these lock-in rings are able to improve the rejection of the residual offset by 20-30 dB, leading to a total rejection of the unpolarized component of about 50-60 dB. Some results will be shown in the Section 3.

2.3. Thermal Instabilities

Thermal instabilities can generate deviations from the ideal behaviour. In fact, all of the elements generating offset are sensitive to temperature variations, so that thermal fluctuations induce variations in the offset and, in turn, in the data.

A way to evaluate the impact on the data is the use of transfer functions H providing the fluctuations $\Delta(Q + jU)$ on the data when the physical temperature varies of ΔT:

$$\Delta(Q + jU) = H\,\Delta T. \tag{9}$$

Ref. 28 provides the H expressions for a correlation scheme with respect to the antenna device parameters. Applied to the 32 GHz receiver of BaR-SPOrt, they give the following values for the transfer functions of the two thermal environments:

$$H^{\mathrm{horn}} \sim 6 \times 10^{-5}, \tag{10}$$

for the warm stage (horn), and

$$H^{\mathrm{cold}} \sim 8 \times 10^{-4} \tag{11}$$

for the cold one.

These are very low levels, and are due to the low offset value of our correlation architecture. We will see in Section 4 that these values, combined with the high thermal stability of the BaR-SPOrt design, ensure a negligible contamination on the data.

3. TESTS OF THE RECEIVER SUBSYSTEMS

The construction of the 32 GHz radiometer is almost completed: we have already assembled and tested all the subsystems separately (Warm RF, Warm LF, Antenna System, Optics) and they are now integrated in the whole radiometer for the final tests. In the following we present all of these subsystems together with the relevant results of their tests.

3.1. Primary Optics

The primary optics is the first relevant subsystem. It consists of a on-axis Cassegrain configuration with a 1.8 m primary mirror (see Figure 5). We have measured the surface to check for errors with respect to the ideal

Figure 5. 1.8 m Cassegrain optics of BaR-SPOrt.

parabolic shape. An rms deviation Δz of

$$\Delta z \sim 60\,\mu\text{m} \tag{12}$$

has been found, that corresponds to about $\lambda/160$ at the central frequency of 32 GHz. Thus, the shape of the mirror can be considered practically ideal at the lower frequency of BaR-SPOrt. At 90 GHz this error corresponds to about $\lambda/55$, so that the mirror can provide very good performances even for the second step of the BaR-SPOrt project, when a W-band receiver will substitute the present one. Also the subreflector has been measured: this is even better, featuring an rms error of about 45 μm.

3.2. Antenna System

All the antenna devices have been custom developed by our team to satisfy the requirements in terms of purity in Q and U mesurements.

The vacuum window, which allows the feed to observe the sky, has been selected to limit the induced instrumental polarization. Tests on several materials have been performed and a 3.3 mm thick teflon layer has been finally adopted (see Ref. 27 for analysis and tests).

The feed horn has been designed and built to ensure a cross-polarization better than 40 dB and a return loss better than 35 dB along all the bandwidth. Figure 6 reports the measured values.

To calibrate the system, we developed an innovative method based on the insertion of three known signals.[29] The marker injector, located between horn and polarizer, has a symmetric design to minimize the impact on the polarized signal coming from the feed horn. Designed in multi-mode regime, it shows high performances in terms of insertion loss (better than 0.025 dB) and return loss (of the order of 40 dB).

The devices of the cold stage (polarizer and OMT) are now assembled in the cryogenic box of the instrument (Figure 7). The main performaces of these components have been already discussed in Section 2 and allow the receiver to limit the offset generation, ensuring the required high stability of the system.

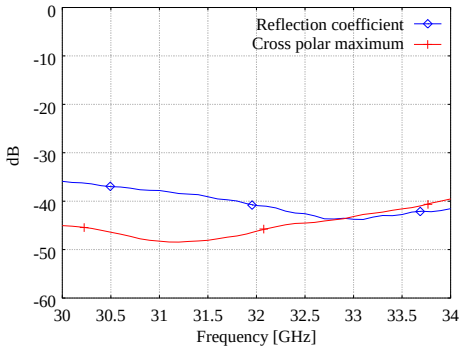

Figure 6. Return loss and maximum of the cross-polar pattern of the 32 GHz horn.

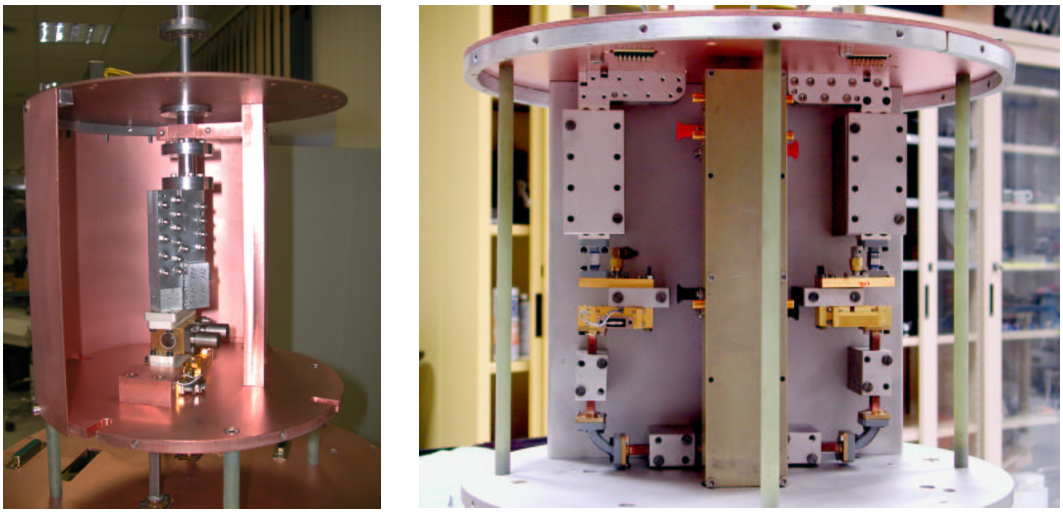

Figure 7. Cold (left) and warm (right) stages of the receiver. The pictures show all the devices assembled before the wiring.

3.3. Warm RF Stage and LF Electronics

Figure 7 shows the warm stage of the system. This stage contains the core of the receiver: the Correlation Unit based on the HPD, diodes and differential amplifiers. This unit, together with the lock-in system, has been fully tested, expecially to check its capability to reject the contamination from the unpolarized component. Our tests show that the HPD alone (lock-in not activated) performs a 35 dB rejection, i.e. when an unpolarized signal enters the receiver, the CU generates a correlated signal whose value is about 3×10^{-4} lower.

These high performances are enhanced by the lock-in system: with this system activated we have measured a 52 dB total rejection. However, this represents just an upper limit of the real performances, because our tests were limited by the noise. Actually, we checked that the lock-in alone is featured by a 28 dB rejection capability, so that we expect an effective rejection of the whole CU better than 60 dB.

4. INTEGRATED RECEIVER AND THERMAL TESTS

As mentioned before, all of the previous subsytems have been integrated in the cryostat and the whole receiver is now under test. Figure 7 shows the cold stage assembled in the cryo-box and the warm section attached to the thermal shield which provides the thermal control.

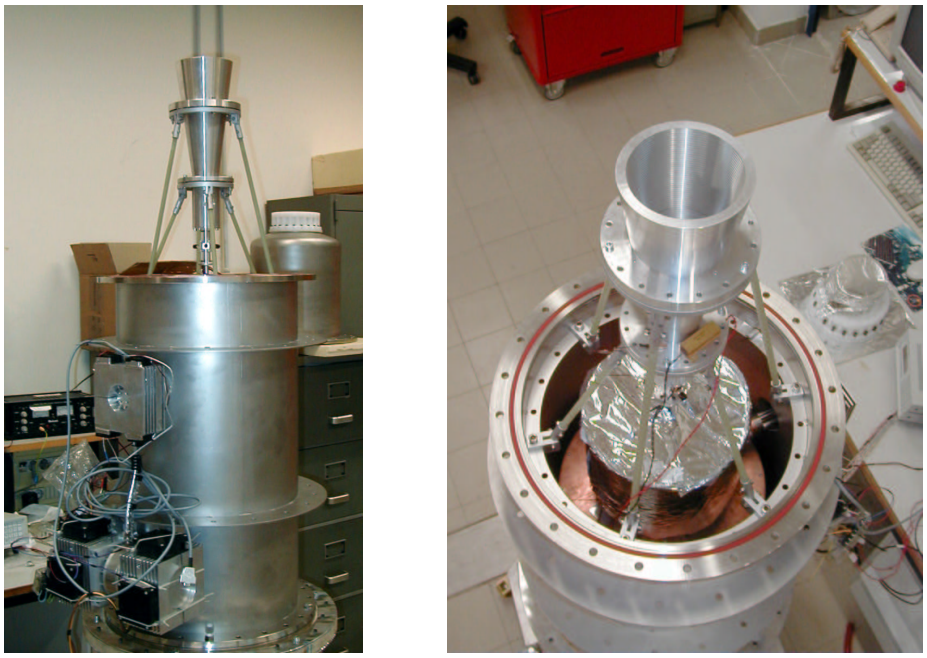

Figure 8. BaR-SPOrt receiver at 32 GHz. In the picture on the right is well visible the MLI covering the cryo-box.

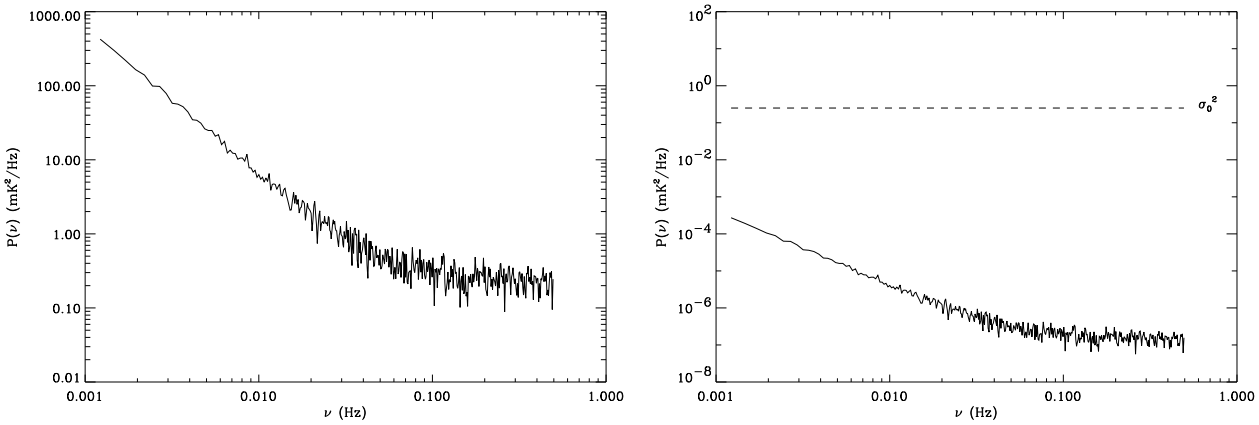

Figure 9. Left: Power spectrum of the thermal fluctuations of the cold stage. Right: Power spectrum of the noise induced by the thermal fluctuations on the data (solid) together with that of the receiver noise (dashed).

To date we have completed a first run of thermal tests. Figure 8 shows the receiver before being closed with the upper part of the cryostat. In particular, the picture on the right shows the cold-box covered by the Multi Layer Insulation (MLI), which shields the box from the radiative heat exchange.

The test were successful, with the cold-box cooled at the nominal temperature and with a proper stability. The box has mantained a fixed temperature within $\pm$ 0.1 K for about one day and within $\pm$ 0.005 K in about 1000 seconds (see Ref. 21 for further details).

Figure 9 shows the power spectrum of the thermal fluctuations of the polarizer which, being the cold component farthest from the cold finger, represents the worst controlled device. Scaled by $(H^{\rm cold})^2$, it provides the power spectrum of the noise induced on the data by the thermal fluctuations themself (see Figure 9). The

comparison with the white noise expected for the radiometer (noise system temperature of LNAs and antenna assembly) clearly shows that the noise induced by thermal fluctuations gives a negligible contribution to the total noise on scan-period time-scales (minutes), time over which the instability can be removed by destriping techniques. This gives us the confidence that our thermal design provides the proper stability for the measurement of the weak CMBP signal, without further contributions to the total noise.

Similarly, we also tested the capability of the thermal control of the warm sections. The results are similar to the cold stage ($\pm$ 0.1 K in about one day; $\pm$ 0.005 K in about 1000 seconds, see Ref. 21), allowing the requested high thermal stability also in this case. In fact, the value of $H^{\rm horn}$ translates the 1000 s variations into ~ 0.3 μK for the data, well below the few μK expected for the sky signal.

ACKNOWLEDGMENTS

BaR-SPOrt is a project funded by the Italian Space Agency (ASI) and partially supported by the National Project for Research in Antarctica (PNRA). We acknowledge the use of the CMBFAST package.

REFERENCES

1. Bennett C., et al., *ApJS* **148**, 1, 2003.
2. http://wmap.gsfc.nasa.gov
3. http://lambda.gsfc.nasa.gov/product/map/
4. http://astro.estec.esa.nl/SA-general/Projects/Planck/planck.html
5. Zaldarriaga M., Spergel D. N., Seljak U., *ApJ* **488**, 1, 1997
6. Zaldarriaga M., *ApJ* **503**, 1, 1998.
7. Cen R., *ApJ* **519**, 12, 2003.
8. Spergel D.N., et al., *ApJS* **148**, 175, 2003.
9. Kosowsky A., *New Astron. Rev.* **43**, 157, 1999.
10. Kamionkowski M., Kosowsky A., *PRD* **57**, 685, 1998.
11. Kinney W.H., *PRD* **58**, id. 123506, 1998.
12. Kovac J., et al., *Nature* **420**, 772, 2002.
13. Kogut A. et al., *ApJS* **148**, 161, 2003.
14. Cortiglioni S. et al., *New Astron.* **9**, 297, 2004.
15. Sbarra C., Carretti E., Cortiglioni S., Zannoni M., Fabbri R., Macculi C., Tucci M., *A&A* **401**, 1215, 2003.
16. Hedman M.M., Barkats D., Gundersen J.O., McMahon J.J., Staggs S.T., Winstein B., *ApJ* **573**, L73, 2002.
17. Keating B.G., O'Dell C.W., Gundersen J.O., Piccirillo L., Stebor N.C., Timbie P.T., *ApJS* **144**, 1, 2003.
18. Farese P.C., et al., *ApJ*, submitted, astro-ph/0308309.
19. Barkats D., *New Astron. Rev.* **47**, 1077, 2003.
20. Peverini O.A., Baralis M., Tascone R., Trinchero D., Olivieri A., Carretti E., Cortiglioni S., in *Astrophysical Polarized Backgrounds*, *AIP Conf. Proc.* **609**, 177, 2002.
21. Zannoni M., et al., *this volume*, 2004.
22. Wollack E.J., *Rev. Sci. Instrum.* **66**, 4305, 1995
23. Wollack E.J., Pospieszalski M.W., *IEEE MTT-S Digest 1998*, p. 669, 1998
24. Carretti E., et al.; in *Polarimetry in Astronomy*, ed. S. Fineschi, SPIE Conf. Proc. **4843**, 305, 2003.
25. Carretti E., Tascone R., Cortiglioni S., Monari J., Orsini M., *NewA* **6**, 173-187, 2001 (*astro-ph*/0103318).
26. Peverini O.A., et al., *this volume*, 2004.
27. Macculi C., et al., *this volume*, 2004.
28. Carretti E., Zannoni M., Macculi C., Cortiglioni S., Sbarra C., *A&A*, submitted, 2004.
29. Baralis M., et al., in *Astrophysical Polarized Backgrounds*, *AIP Conf. Proc.* **609**, 257, 2002.